Feet on the ground: Physical support of the inner retina is a strong determinant for cell survival and structural preservation in vitro.

Taylor, Linnéa; Arnér, Karin; Holmgren Taylor, Ingrid; Ghosh, Fredrik

Published in:
Investigative Ophthalmology & Visual Science

DOI:
10.1167/iovs.13-13535

2014

Feet on the ground: Physical support of the inner retina is a strong determinant for cell survival and structural preservation in vitro

Linnéa Taylor, Karin Arnér, Ingrid Holmgren Taylor, Fredrik Ghosh
Department of Ophthalmology, Lund University Hospital, Lund, Sweden

Corresponding author:
Linnéa Taylor
Department of Ophthalmology
Lund University Hospital
S-22184 Lund, Sweden
phone:+46 46 2220752
fax: +46 46 2220774
e-mail: linnea.taylor@med.lu.se

Supported by: The Faculty of Medicine, University of Lund, The Swedish Research Council, The Princess Margaretas Foundation for Blind Children, Marianne and Marcus Wallenbergs Foundation.

ABSTRACT

Purpose: The purpose of this study was to explore the importance of local physical tissue support for homeostasis in the isolated retina.

Methods: Full-thickness retinal sheets were isolated from adult porcine eyes. Retinas were cultured for 5 or 10 days using the previously established explant protocol with photoreceptors positioned against the culture membrane (porous polycarbonate) or the Müller cell endfeet and inner limiting membrane (ILM) apposed against the membrane. The explants were analyzed morphologically using hematoxylin and eosin staining, immunohistochemistry, TUNEL labeling, and transmission electron microscopy (TEM).

Results: Standard cultures displayed a progressive loss of retinal lamination and extensive cell death, with activated, hypertrophic Müller cells. In contrast, explants cultured with the ILM facing the membrane displayed a maintenance of the retinal laminar architecture, and a statistically significant attenuation of photoreceptor and ganglion cell death. TEM revealed intact synapses as well as preservation of normal cellular membrane structures. Immunohistochemistry showed no signs of Müller cell activation (GFAP), with maintained expression of important metabolic markers (GS, bFGF).

Conclusion: Providing physical support to the inner but not the outer retina appears to prevent the tissue collapse resulting from perturbation of the normal biomechanical milieu in the isolated retinal sheet. Using this novel paradigm, gliotic reactions are attenuated, and metabolic processes vital for tissue health are preserved which significantly increases neuronal cell survival. This finding opens up new avenues of adult retinal tissue culture research, and increases our understanding of pathological reactions in biomechanically related conditions in vivo.

INTRODUCTION

In the living eye, the neuroretina is stretched and fixated against the interior wall by means of hydrostatic pressure and adhesion with the posterior vitreous membrane and the retinal pigment epithelium [1-2]. Interestingly, conditions in which the mature neuroretinal sheet is removed from these normal forces such as retinal detachment in vivo and explant cultures in vitro, elicit similar tissue reactions i.e gliosis and neuronal degeneration [3-4]. We have previously explored the relationship between biomechanical force and retinal homeostasis and have shown that when in vivo tension is emulated in vitro, by laterally stretching the tissue, gliosis and neuronal cell death in adult porcine explants are significantly attenuated [5]. However, the exact mechanism behind this phenomenon remains to be explained. Intriguingly, Müller cells have recently been shown to possess mechanosensory and mechanoregulatory properties [2, 6-7]. The Müller cells, previously viewed in this context as a passive scaffold for the retinal neurons, are aptly placed to act as mechanosensors, as they vertically span the retinal layers from the outer to the inner limiting membrane. The laminar architecture as well as cell density contribute to the differential viscoelastic properties of the retina, which vary not only from center to periphery, but from inner to outer border. The outer retina consists of pliable inner and outer segments, which provide little in form of structural stability, whereas at the inner retinal perimeter, the Müller cells form stiff endfeet rich in mechanosensitive ion channels indicating that the biomechanical responsive element of the retina is located in this region.

The retinal organ culture paradigm has been in use since the early 1930's [8], and has since been employed as a model to study the central nervous system in a variety of species. The most common method entails dissecting the retinal sheet free from the surrounding tissues, and placing it with the outer layers apposed to a culture membrane in medium for incubation

[9-11]. This polarity of the retinal tissue in culture was most likely chosen due to the high metabolic rate of the photoreceptors, with the rationale that survival of these cells would be enhanced by the close proximity to the culture medium. In addition, it was believed that the support provided by the culture membrane would mimic physical RPE-outer segment interaction in vivo. This approach has been used successfully for the study and modulation of immature tissue which has been found to survive well with several signs of normal development [9-13]. In contrast, as mentioned above, isolated adult retinal sheets cultured under standard conditions, display gliosis and neuronal degeneration very early [14-17]. The discrepancy of cell survival in vitro depending on stage of maturity is well established, but not yet fully understood.

For the present paper, based on our previously published results on the importance of a biomimetic physical environment for retinal homeostasis, we hypothesize that apposing the comparatively stiff adult inner retina against the non-elastic culture membrane may provide better stability compared with traditional explants in which the culture membrane is apposed to the outer retina. Thus, an improved physical interaction between the tissue and culture membrane may help to restore the collapsed network structure in the isolated retinal sheet removed from the normal stabilizing forces present in the eye. We have thus cultured adult retinal explants ”upside down” i.e with the inner limiting membrane facing the culture membrane, and compared their neuronal survival and Müller cell reactions with conventionally cultured counterparts.

MATERIAL AND METHODS

Tissue Culturing

All proceedings and animal treatment were in accordance with the guidelines and requirements of the government committee on animal experimentation at Lund University and with the ARVO statement on the use of animals in ophthalmic and vision research. Eyes were harvested from adult pigs aged between 4-6 months euthanized by an overdose of sodium pentobarbital, (Apoteket, Umeå, Sweden). The neuroretinas were removed using the method described previously by Engelsberg and Ghosh in 2007 [12]. To summarize, the eyes were enucleated immediately after sacrifice and immersed in CO2 –independent medium (Invitrogen, Paisley, UK). The anterior segment was excised by a sharp incision in the pars plana and cut 360 degrees. The vitreous was removed in one piece by carefully pulling it from the eyecup using sterilized tissue paper. The neuroretinas were gently dissected free from the pigment epithelium with microforceps and the optic nerve head was carefully cut using microscissors. Each neuroretina was sectioned into 6 pieces, measuring approximately 6 mm^2. In total, 18 eyes from 9 animals were used, yielding 91 specimens for culture and 2 eyes serving as a normal adult in vivo controls. The 91 neuroretinal pieces were explanted onto Millicell- PCF 0.4 μm culture plate inserts (Millipore, Billerica, MA, USA; Fig. 1), with either the photoreceptors (standard protocol; CT) or with the ILM positioned against the culture membrane, providing the explants with inner retinal support (IRS; Fig. 2). Specimens were cultured in 1,5 ml DMEM/F12 (Invitrogen) supplemented with 10% fetal calf serum (Sigma-Aldrich, St Louis, MO, USA) as well as a cocktail containing 2 mM L-glutamine, 100 U/ml penicillin and 100 ng/ml streptomycin (Sigma Aldrich) for 5 and 10 days. The explants were maintained in an incubator at 37 °C at 95% humidity and 5% CO2. The medium was exchanged every second day.

Histology

Histological examinations were performed as previously described [12], and only briefly recapped here. After culturing, the explants were fixed in 4% paraformaldehyde in 0.1M phosphate buffer, pH 7.2 for 2h in 4 °C. The normal adult in vivo controls were fixed immediately after harvest using the same paraformaldehyde concentration for 4h in 4 °C. The explants were then infiltrated with 0.1M Sörensens medium with increasing concentrations of sucrose up to 25%. They were then embedded in egg albumin/gelatine medium for cryosectioning at -20 °C with a section thickness of 12 µm. For light microscopy, every 10th slide was stained with hematoxylin and eosin. For immunohistochemical labeling, adjoining slides with sections originating from the center of the explants (the area centralis in the normal control) were chosen. The specimens were rinsed 3 times with PBS containing 0.1% Triton- X, and then incubated with PBS containing 0.1% Triton-X and 1% bovine serum albumin (BSA) for 20 minutes at room temperature. After this, the specimens were incubated overnight at 4 °C with the respective primary antibody (Table 1). In the double labeling for GS/bFGF, both primary antibodies were added at this stage. The specimens were then rinsed in PBS-Triton-X (0.1%), and incubated for 45 minutes with a secondary fluorescein isothiocyanate (FITC) or Texas Red-conjugated antibody (Table 1). In the double labeling for GS/bFGF, both secondary antibodies were added at this stage. The specimens were then mounted in Vectashield mounting medium with 4',6-diamidino-2-phenylindole (DAPI; Vector laboratories Inc., CA, USA). Negative control experiments were performed as above, replacing the primary antibody with PBS containing 0,1% Triton-X and 1% BSA. Normal porcine adult retina was used as a positive control.

For transmission electron microscopy, cultured explants were fixed in 4% glutaraldehyde in phosphate buffer over night at 4°C. The fixation was followed by repeated rinsing in caco-

dylate buffer, after which the explants were post-fixed in 1% osmium tetroxide. The explants were dehydrated using increasing concentrations of ethanol, and embedded in Epon resin. Ultrathin sections (50nm) were then taken from the central part of the specimens for transmission electron microscopy.

Microscopy and image analysis

The histological sections and immunohistochemically labeled specimens were examined using an epifluorescence microscope (Eclipse E800; Nikon, Tokyo, Japan) equipped with an Olympus digital camera system (Olympus, Tokyo, Japan) and a digital acquisition system (DP 70; Olympus, Tokyo, Japan). Photographs were taken at each end of the section, and in the center. Transmission electron microscopy specimens were examined using a 120 kV JEOL 1230 (JEOL, Herts, UK), equipped with a cooled, high-resolution digital camera (Gatan, Abingdon Oxon, UK). Images were viewed and processed using Photoshop (Adobe Systems, Mountain View, CA).

Statistical Analysis

Immunohistochemically labeled sections were used to statistically quantify survival of individual cell types. One central section per cultured specimen was analyzed for TUNEL, rhodopsin, and NeuN labeling, along with one section per in vivo reference eye. In vivo reference tissue and cultured specimens were processed in the same batch for each immunohistochemical labeling. Three photographs were obtained from the sections, and labeled cells (TUNEL and NeuN) and labeled cell rows in the ONL (rhodopsin) were counted at 40x magnification. Normal control tissue and cultured specimens were processed in the same batch for each immunohistochemical labeling. Data were analyzed using ANOVA with a Tukey post hoc test (GraphPad InStat; GraphPad Software, San Diego, CA). Raw data from cell counts were used

to generate mean values for each of the groups. Values of $P < 0.05$ were considered significant.

RESULTS

In vivo controls

The overall morphology and immunohistochemical characteristics of the normal adult porcine retina has been well described previously but will be summarized here [4-5, 12-18]. Hematoxylin and eosin staining of in vivo controls revealed clearly defined nuclear and plexiform layers as previously described (Fig. 3A). Rhodopsin immunohistochemistry revealed strong labeling of outer segments at the outer border of the specimen, as well as weaker labeling of inner segments and photoreceptor cell bodies (Fig. 3B). Transducin labeling showed cone photoreceptor cell bodies in the outer part of the outer nuclear layer (ONL), as well as labeled processes in the outer plexiform layer (OPL; Fig. 3C). Strong labeling was also present in cone bipolar cell perikarya located in the inner nuclear layer (INL), and in their processes vertically spanning the INL and inner plexiform layer (IPL). NeuN labeling showed a multitude of large cell bodies in the ganglion cell layer (GCL) corresponding to ganglion cells (Fig. 3D). Strong labeling of synaptic vesicles in both the OPL and IPL were seen using the synaptophysin antibody. (Fig. 3E). Specimens labeled with GFAP displayed strong labeling of astrocytes and Müller cell endfeet at the innermost part of the specimens (Fig. 3F). Weak labeling of vertical Müller cell fibers was present throughout the retina, which is normal for this species [18]. Double labeling with GS and bFGF showed diffuse GS expression throughout the retinal layers, with bFGF labeling of Müller cell bodies in the INL and amacrine cells in the GCL, which is normal for this species (Fig. 3G) [18].

Cultured explants

Overview morphology and apoptosis

Hematoxylin and eosin staining of 5 and 10 days in vitro (DIV) inner retinal support (IRS) specimens revealed an overall retained laminar architecture with well-populated nuclear lay-

ers. The ILM appeared to be adherent to the culture membrane, although no growth into the membrane was observed. Inner and outer segments appeared present, albeit slightly disorganized (Fig. 4A and B). The standard cultured counterparts (CT), in contrast, contained multiple vacuoles at 5 DIV with a multitude of pyknotic cells present in all nuclear layers (Fig. 4C). No inner or outer segments could be identified, with cellular debris lining the outer border toward the culture membrane. At 10 DIV the ONL appeared degenerated, with some remaining cells in the INL and GCL (Fig. 4D). Subretinal Müller cell growth was observed lining the outer border of the specimen.

TUNEL labeling revealed apoptotic cells in the ONL and GCL in 5 DIV IRS explants (Fig. 4E). Similarly, at 10 DIV, labeled cells were observed in the ONL (Fig. 4F). CT specimens displayed a multitude of labeled cells in all nuclear layers after 5 DIV (Fig. 4G). After 10 DIV, scattered labeled cells were present, mostly in the remaining outer retina (Fig 4H). Statistical analysis revealed significantly fewer labeled cells in 5 DIV IRS specimens compared with their CT counterparts ($p<0,001$; Fig. 5A). No significant difference was found between IRS specimens and CT specimens after 10 DIV.

Immunohistochemistry

IRS specimens labeled with rhodopsin revealed labeling of rod photoreceptors in the entire ONL with somewhat higher labeling intensity corresponding to the inner and outer segment area at both 5 and 10 DIV (Fig. 6A and B). CT specimens revealed strong labeling of disorganized structures in the outer part of the specimen at 5 DIV (Fig. 6C). At 10 DIV, strong labeling of scattered structures and isolated cell bodies at the outer border was observed (Fig. 6D). Statistical analysis of rhodopsin-labeled cell rows revealed a significant preservation of the ONL of IRS specimens at both 5 and 10 DIV compared with their CT counterparts ($p<0,001$; Fig. 5B). Transducin labeling of 5 DIV IRS specimens revealed cone photoreceptor

cell bodies, inner and outer segments in the outer ONL as well as cone pedicles in the OPL (Fig. 6E). Labeling was also found in a population of bipolar cells in the INL. A similar labeling pattern was observed in the 10 DIV specimens, but cones as well as bipolar cells were not as strictly organized. (Fig. 6F). In contrast, 5 DIV CT explants almost completely lacked the normal organized morphology displaying scattered labeled cells in the ONL (Fig. 6G). After 10 DIV only isolated labeled cone cells remained whereas labeling of cone bipolar cells was still present (Fig. 6H).

NeuN labeling of IRS specimens revealed numerous large cell bodies in the GCL at both 5 and 10 DIV, with significantly more labeled cells than in their CT counterparts ($p<0.001$ at 5 DIV and $p<0.01$ at 10 DIV respectively; Fig.5 C; Fig. 7A-D). Synaptophysin labeling of 5 and 10 DIV IRS specimens revealed strong labeling of synaptic vesicles in the OPL, with slightly weaker labeling of the IPL (Fig. 7E and F). In contrast to normal in vivo controls, autofluorescence was present in the inner and outer segment area. The corresponding 5 DIV CT specimens displayed strong labeling of the IPL and OPL, with both layers appearing more disorganized compared with their IRS cultured counterparts (Fig. 7G). After 10 DIV, only isolated labeling was found in the highly disorganized OPL, whereas stronger labeling was present in the thin, vacuolized IPL (Fig. 7H).

GFAP labeling of IRS specimens cultured for 5 and 10 DIV revealed strong labeling at the inner border, with weaker labeling of vertical fibers, comparable to that found in the in vivo controls (Fig. 8A and B). No gliotic remodeling was evident. Corresponding CT specimens revealed an upregulation of GFAP expression with high intensity labeling present throughout the sections (Fig. 8C and D). Progressive gliotic remodeling was observed from 5 to 10 DIV, where the 10 DIV specimens displayed folding and subretinal fibrotic growth.

GS/bFGF double labeling of IRS specimens revealed strong labeling of GS at the inner border of the specimen at 5 DIV, with slightly weaker labeling present throughout the section, comparable to the in vivo controls (Fig. 8E). At 10 DIV, strong GS labeling was present throughout the Müller cells (Fig. 8F). bFGF labeling of both 5 and 10 DIV specimens revealed a multitude of Müller cell nuclei in the INL as well as scattered amacrine cells in the GCL. Labeling of CT counterparts revealed a down-regulation of GS at both 5 and 10 DIV (Fig. 8G and H). An upregulation of bFGF in cells located mostly in the INL, but also at the innermost and outermost borders of the specimen was found at 5 DIV. At 10 DIV, only scattered cells were labeled with bFGF.

Ultrastructure

Transmission electron microscopy revealed intact inner and outer segments in 5 DIV IRS specimens, with a well-delimited OLM (Fig. 9A and B). Ribbon synapses with intact triads were present, as well as conventional synapses (Fig. 9C). In 5 DIV IRS specimens, intact ribbon synapses as well as electrical synapses were present in the OPL (Fig. 9D and E). Both ribbon synapses and conventional synapses were found in the IPL (Fig. 9F and H). At the inner border, Müller cell endfeet were found with the intact ILM facing the culture membrane (Fig. 9H). No Müller cell sprouting into the membrane pores was found.

5 DIV CT specimens showed no intact inner or outer segments, although isolated phagocytosed outer segment debris was found (Fig. 10A). Müller cell growth was present subretinally, with processes sprouting into the culture membrane pores. The ONL appeared disorganized with pyknotic cell bodies present (Fig. 10B). In standard cultured specimens, short, dislocated ribbon synapse structures could be found in the OPL (Fig. 10C) although the OPL appeared to consist mainly of cellular debris (Fig. 10D). Isolated short ribbon synapses and conventional synapses were present in the IPL (Fig 10E and F). The IPL, similar to the OPL, contained cel-

lular debris and electron dense material (Fig. 10G). In the inner part of the explants, large vacuoles were found (Fig. 10H). The ILM appeared intact, although Müller cell growth was present.

IRS specimens cultured for 10 DIV displayed photoreceptor inner segments with occasional outer segment ciliae, as well as an intact OLM (Fig. 11A). No normal outer segments could be found. A multitude of photoreceptor nuclei were present, and their processes could be followed inwards towards the OPL (Fig. 11B) Numerous intact ribbon synapses were present at the inner border of the ONL (Fig. 11C). Large cell bodies were found at the inner border apposed against the culture membrane (Fig. 11D). No Müller cell growth into the membrane was observed. In comparison, CT specimens displayed subretinal gliotic remodeling with Müller cell growth, as well as only a few, shrunken unidentifiable nuclei present (Fig. 11E) Isolated, small photoreceptor nuclei were found in the ONL (Fig. 11F). Pyknotic nuclei were present in the INL, as well as scattered Müller cell nuclei (Fig. 11G). The inner retina appeared highly disorganized with dark, gliotic Müller cell processes lining the inner border (Fig. 11H).

DISCUSSION

Summary

In this study, we used the explant culture paradigm to explore the importance of inner retinal support for tissue homeostasis in adult porcine retina. Based on our previous findings that biomimetically stretching retinal explants significantly extends adult tissue survival time in culture, coupled with the discovery of mechanoreceptors concentrated to the inner retina, we reinvented the traditional culture paradigm through the inversion of the explant, instead using the culture membrane to provide support for the inner retina. Culturing the retina with inner layer support has been reported previously by Wang et al., 2011 [19]. In this video article, Wang and colleagues described cultures of adult porcine retina explanted onto sterile filter paper to facilitate attachment, and found that retinal morphology, investigated using GFAP, propidium iodide and synaptic vesicle protein 2, was preserved for up to 7 days in vitro. In our paper, where we provide support to the inner retina by placing it directly onto the culture membrane and expand the morphological analysis, we can confirm that inner retinal support is of vital importance for structural preservation, synaptic maintenance as well as cell survival and metabolic health in adult retinal cultures.

In contrast to immature tissue, which has successfully been used in culture for many decades, the use of adult retinal tissue in vitro has been limited due to the fact that it can not be kept for extended time periods in culture using standard methods. Due to significant neuronal degeneration and gliosis the time restriction has been 3-4 DIV [3-5, 9-11, 15, 17]. Improved survival of adult rodent retinal tissue has previously been demonstrated on biochemically and structurally modified substrates, indicating that the local biomechanical environment is important for cell health [20]. Using our novel approach, we have shown that these pathological changes can be significantly attenuated by providing mechanical support to the inner retina.

Survival of inner and outer retinal cells.

The culture procedure entails axotomy of retinal ganglion cells, which both in vitro and in vivo, rapidly induces apoptosis [5, 14-15, 17, 21-23]. Several approaches have been explored to minimize the axotomy effect on ganglion cells. One common strategy in vitro is to supplement the medium with neurotrophic factors [17, 22, 25-27]. Despite this treatment, only limited numbers of ganglion cells have been shown to survive, which has at least in part been attributed to a reduced responsiveness to neurotrophins[17, 28-31]. However, even when the expression of neurotrophic receptors is enhanced through cAMP elevation and a cocktail of suitable support factors is delivered, only around 50% of cells can be saved three days after axotomy in vivo [30-31]. We observed a preservation of approximately 40% of ganglion cells in our IRS cultured explants after 5 DIV without using neurotrophic treatment indicating that inner retinal biomechanics may be important for tissue homeostasis.

Another striking pathological alteration in previous experiments involving adult retinal explants takes place in the outer retina [5, 14-17]. The deconstructive process leading to photoreceptor cell death is highly similar in the adult explant culture system and retinal detachment in vivo [32-33]. After detachment, photoreceptors die mainly by apoptosis, which occurs quite rapidly [5, 12, 14-17, 34-35]. In vitro under standard conditions, the degenerative process also progresses quickly, with the majority of the photoreceptors appearing pyknotic after 3-4 DIV [4, 12, 14-15]. In contrast, our specimens cultured with inner retinal support displayed a significantly enhanced photoreceptor survival with several signs of preserved cell health evident in TEM and with immunohistochemical markers. The rapid photoreceptor degeneration observed in traditional cultures and in detached retinas in vivo has largely been attributed to the loss of support from the retinal pigmented epithelium (RPE) and choroidal circulation. However, full-thickness retinal explants cultured using the conventional protocol but with an intact

RPE still display photoreceptor degeneration and gliosis, even when placed in perfusion culture [14-15]. Other indications that these factors may not be an acute concern are found in patients with central serous chorioretinopathy, where the detachment is often left to spontaneously resolve, and in most cases results in only minor vision loss [36]. The high oxygen consumption of the photoreceptors is well known, and the cell survival may therefore be increased by the increased air exposure of the outer layers by the inversion of the explants. However, the preservation of ganglion cells in the IRS specimens as well as our previously published results on significantly preserved photoreceptor health using the standard culture procedure with the addition of biomimetic stretch, indicate that this is not the primary determinant for the increased photoreceptor survival. The significant preservation of the photoreceptors and ganglion cells in our IRS specimens therefore suggest that neither nutritive support from the choroid, oxygen supply or physical interactions between outer segments and RPE are the primary determinants of cell survival in the isolated retinal sheet, but that the biomechanical milieu may in fact be pivotal.

Mechanisms and biomechanics

In vivo, the retina resides in a highly mechanical environment where adhesive, tensile and hydrostatic pressure forces come into play [1, 37-38]. During development, the retinal sheet is passively stretched during expansion of the globe. In the mature eye, it is sandwiched between the posterior vitreous membrane and the RPE, and maintained in a stretched state by the intraocular pressure (IOP) [1, 37-38]. During the culture procedure, the IOP is lost when the eye is opened and the retina is dissected free from the vitreous and the RPE, leading to a loss of tissue tensility and a collapse of the network structure of the tissue (Fig. 12 A-C) [4-5].

The elastic retinal network consists of soft Müller glia interposed with stiffer neuronal cell bodies [39]. The viscoelastic properties of the retina vary not only from center to periphery

but from inner to outer border. Our group has previously demonstrated the importance of preserving the normal retinal lateral tension for explant health in vitro [5]. We found that free-floating cultured explants, which lacked all physical support, displayed rapid disintegration with the majority of cells appearing pyknotic after 2 DIV. Standard cultured explants, placed on the membrane over the pliable inner and outer segments which undergo rapid degeneration, left the explant network structure distorted, and as in the current experiment, quickly became gliotic with extensive neuronal cell death. In comparison, specimens cultured under standard conditions with the addition of biomimetic stretch displayed increased survival of both ganglion cells and photoreceptors as well as an attenuation of the gliotic process for up to 10 days [5]. In the present work we found strikingly similar results by providing the inner retina with mechanical support. Thus, inner retinal support and lateral stretch appears to reproduce a common permissive biomechanical environment with stability of the retinal glioneuronal network as a key factor.

In the retina, the biomechanical scaffolding as well as the biochemical homeostatic upkeep is maintained by the Müller cells. These cells can alter their elasticity and stiffness through up- and downregulation of cytoskeletal intermediary filaments, the most common of which are GFAP and vimentin, thereby altering both the tissue-wide and cellular biomechanical milieu [6, 40-41]. Interestingly, mechanosensory Ca^{2+} ion channels such as TRPV4 are known to be present on Müller cells, particularly on the comparatively stiff and intermediate filament-rich Müller cell endfeet at the inner retinal border [2, 7, 39, 42]. These channels have been shown to respond to changes in cell membrane tensility by Ca^{2+} influx, which in turn can cause upregulation of intermediate filaments in Müller cells [7, 40-45]. Ca^{2+} influx is a common response to mechanical stimuli seen in several types of mechanosensitive cells [6, 46-49]. The presence of TRPV4 channels in the Müller cell endfeet may thus provide the retina

with a sensor of biomechanical changes. During injury and disease, the Müller cells become activated, losing their metabolic functions and structural integrity [40-41, 50]. These gliotic changes lead to a highly detrimental environment for the neuronal cells, thereby accelerating cell death [40-42, 51]. Because of this, gliosis has been considered the limiting factor behind long-term cultures of adult retinal explants using the standard method [5, 12, 14-17]. In our standard cultured explants, Müller cell hypertrophy and subretinal growth was widespread with a multitude of glial processes sprouting into the culture membrane. The IRS specimens, in contrast, showed no signs of Müller cell activation, with a preservation of GS as well as bFGF expression. The lack of gliotic response thus may allow the Müller cells to preserve their normal regulatory and metabolic functions, which in turn promotes neuronal health [40-41].

Conclusion

In this paper we have explored the effects of biomimetic structural stability on adult retinal explants. Specimens cultured with inner retinal support displayed a significant preservation of photoreceptors and ganglion cells at 5 and 10 DIV, with a profound attenuation of the gliotic response. Control explants cultured using the standard culture method displayed extensive degenerative changes in a deconstructive process similar to that observed in retinal detachment. The herein presented relationship between biomechanical environment and retinal cell health enhances possibilities of using adult retinal tissue for culture related research, and may increase our understanding of pathological events in biomechanically related conditions in vivo.

FIGURE LEGENDS

Fig 1: Scanning electron microscopy image of the culture well membrane. Porous polycarbonate culture membrane. Pore size 0.4 μm. Scale bar 2 μm.

Fig 2. Illustration of the positioning of the retina on the culture membrane in the different culture groups. Illustration of the inner retinal support (IRS) explant, cultured with the inner limiting membrane facing the culture membrane (A) compared with the standard explant (CT) in which the photoreceptor outer segments are apposed to the membrane (B).

Fig 3: Adult porcine in vivo controls. A Hematoxylin and eosin staining (H&E) B-G Immunohistochemical labeling. A) H&E labeling shows a clearly defined laminated architecture, with well populated nuclear layers. B) Rhodopsin labeling of rod photoreceptors show strong labeling in the rod outer segments, with weaker labeling present in the inner segments and rod photoreceptor nuclei. C) Transducin labeling of cone photoreceptors and a population of bipolar cells display strong labeling of a row of cone cell bodies in the outer ONL, as well as in cone pedicles in the inner ONL. Labeling is also observed in cone bipolar cell bodies in the inner INL, as well as in vertical processes in the OPL and IPL. D) NeuN labeling of ganglion cells display numerous labeled cells of ganglion cell morphology in the GCL. E) Synaptophysin labeling of synaptic vesicles show strong labeling present in the OPL and IPL. F) GFAP labeling of Müller cells and astrocytes show labeling of thin vertical Müller cell fibers, mainly in the inner part of the specimen, as well as horizontal fibers and astrocytes in the NFL. G) GS/bFGF double labeling reveals strong GS labeling (red) present in the Müller cells throughout the specimen. bFGF labeling (green) is present in the Müller cell nuclei in the inner nuclear layer (INL) as well as in displaced amacrine cells located in the inner part of the specimen. Scale bar 30 μm.

Fig 4: Hematoxylin and eosin staining of cultured retinal explants and TUNEL labeling of apoptotic cells. A-D Hematoxylin and eosin. E-H TUNEL labeling. A) IRS specimens cultured for 5 days in vitro (DIV) display a preservation of the laminated architecture, with the nuclear layers appearing well populated. B) IRS specimens cultured for 10 DIV retain the retinal laminar morphology, with slight thinning of the nuclear layers compared with 5 DIV specimens. C) CT explants display an edematous, dissolving laminar architecture after 5 DIV, with pyknotic cells present in all nuclear layers. D) 10 DIV CT specimens display an almost complete loss of nuclei from the outer nuclear layer (ONL), a thin INL, and significant subretinal growth. The specimens appear thinner than their 5 DIV counterparts. Scale bar 25 μm. E) IRS specimens cultured for 5 DIV display labeled cells in all three nuclear layers. F) Similarly, IRS specimens cultured for 10 DIV display labeled cells in all three nuclear layers. G) CT explants display a multitude of labeled cells throughout the specimen after 5 DIV. H) After 10 DIV CT specimens scattered labeled cells, mostly in the outer layers. Scale bar 25 μm.

Figure 5: Statistical analysis of immunohistochemically labeled cells. A) TUNEL-labeled cells per image. Significantly fewer labeled cells were found in 5 DIV IRS specimens compared with their CT counterparts ($p<0.001$). No significant difference was found between the groups at 10 DIV. Error bars SEM. B) NeuN-labeled cells per image. Significantly more NeuN-labeled ganglion cells were found in IRS specimens at both 5 DIV ($p<0.001$) and 10 DIV ($p<0.01$) compared with their CT counterparts. Error bars SEM. C) Rho-labeled cell rows per image. A significant preservation of rhodopsin-labeled photoreceptor cell rows was

found in IRS specimens at both time points compared with the CT cultured specimens ($p<0.001$). Error bars SEM.

Fig 6: Immunohistochemical labeling of rod and cone photoreceptors in cultured adult porcine retinal explants. A-D Rhodopsin labeling of rod photoreceptors. E-H Transducin labeling of cone photoreceptors. A) IRS specimens cultured for 5 DIV display strong rhodopsin labeling of rod inner and outer segments, with weaker labeling of the rod photoreceptor nuclei in the ONL. B) Rhodopsin labeling of 10 DIV IRS specimens shows strong labeling rod inner and outer segments as well as labeling of the rod photoreceptor nuclei in the ONL similar to that observed in the 5 DIV counterparts. C) CT specimens cultured for 5 DIV display strong labeling of disorganized rod photoreceptor nuclei in the outer part of the specimen, as well as what appears to be inner and outer segment debris at the outer border. D) 10 DIV CT specimens display strong labeling of a scattered, displaced rod photoreceptors in the outer part of the section. No inner or outer segments could be identified. E) IRS specimens cultured for 5 DIV display strong labeling of numerous cone photoreceptors in the outer ONL, with strong labeling of the cone pedicles in the inner ONL. Weak labeling is present in the cone bipolar cells. The labeling pattern is similar to that observed in the in vivo specimens. F) 10 DIV IRS specimens display labeling comparable to that found int their 5 DIV counterparts. G) CT specimens cultured for 5 DIV display strong labeling of a few cell bodies located in the ONL, as well as cone bipolar cells. H) In 10 DIV CT specimens, only isolated cells bodies are labeled, with stronger labeling of cone bipolar cells spanning the inner layers. Scale bar 25 μm.

Fig 7: Immunohistochemical labeling of ganglion cells and synapses in cultured adult porcine retinal explants. A-D NeuN labeling of ganglion cells. E-H Synaptophysin labeling of synaptic vesicles. A) IRS specimens cultured for 5 DIV display strong NeuN labeling of numerous large cells of ganglion morphology in the GCL at the innermost part of the section. B) 10 DIV IRS specimens display labeling comparable to that found int their 5 DIV counterparts. C) CT specimens cultured for 5 DIV display strong labeling of a few large cells located in the GCL corresponding to ganglion cells. D) In 10 DIV CT specimens, only isolated NeuN-labeled cells could be found. Autofluoresencent debris are present in the outer ONL. E) 5 DIV IRS specimens labeled with synaptophysin show strong labeling of the OPL, with slightly weaker labeling of the ILP. F) A similar labeling pattern is seen after 10 DIV. G) In CT specimens, strong labeling is present in the thin and disorganized OPL and IPL at 5 DIV. H) At 10 DIV, only isolated labeling is found in the highly disorganized OPL, with strong labeling present in the thin vacuolized IPL of CT specimens. Scale bar 25 μm.

Fig 8: Immunohistochemical labeling of Müller cells in cultured adult porcine retinal explants. A-D GFAP labeling of Müller cells and astrocytes. E-H GS(red)/bFGF(green) double labeling of Müller cells and displaced amacrine cells. A) 5 DIV IRS specimens display strong GFAP labeling of the innermost border of the section, corresponding to the Müller cell endfeet, as well as some weaker labeling of vertical fibers present in the inner part of the section. B) 10 DIV IRS specimens display labeling similar to that of their 5 DIV counterparts, with weaker labeling of vertical fibers in the inner retina. C) 5 DIV CT specimens display strong labeling of thick, hypertrophied Müller cell fibers throughout the specimen. D) 10 DIV CT specimens display strong GFAP labeling of hypertrophied and disorganized Müller cell fibers throughout the specimen, with subretinal growth evident at the outer border. E) IRS specimens cultured for 5 DIV display strong GS labeling of Müller cells at the inner part of the section, with weaker labeling in the outer parts. bFGF labeling is present in the Müller cell

nuclei located in the INL as well as in displaced amacrine cells in the inner part of the specimen. F) GS labeling of 10 DIV IRS specimens shows strong labeling of Müller cells throughout the section. Strong bFGF labeling is present in Müller cell nuclei in the INL as well as in amacrine cells in the innermost part of the specimen. G) 5DIV CT specimens display weak GS labeling of Müller cell fibers, and bFGF labeling of Müller cell nuclei in the INL and the occasional displaced amacrine cell in the inner part of the section. H) 10 DIV CT specimens display weak GS labeling in horizontal Müller cell fibers at the outer border, and bFGF labeling of large, displaced Müller cell nuclei scattered throughout the section. Scale bar 25 µm.

Fig 9: Transmission electron microscopy of 5 DIV adult porcine retinal explants cultured with inner retinal support. Layer morphology and synapses. A) IRS specimens display intact photoreceptor inner and outer segments (IS and OS). The photoreceptor cilia appear intact, and the IS mitochondria appear healthy. B) IRS specimens show a well delimited outer limiting membrane (OLM) with a multitude of photoreceptor nuclei (PR) present in the ONL. C) Intact ribbon synapses were found in the outer plexiform layer (OPL; arrows) in IRS specimens. D) An intact ribbon synapse in the OPL. E) An electrical synapse in the OPL. F) A ribbon synapse present in the inner plexiform layer (IPL). G) An intact conventional synapse in the IPL. H) IRS specimens display an intact ILM apposed against the culture membrane (MEM). Scale bars A-C 2µm, H 0.5µm. Scale bar D-G 0.5µm.

Fig 10: Transmission electron microscopy of 5 DIV standard cultured adult porcine retinal explants. Layer morphology and synapses. A) CT specimens show subretinal müller cell growth (arrow) along and into the pores of the culture membrane (MEM), with no identifiable photoreceptor IS evident. The occasional phagocytosed outer segment (OS) is present. B) Isolated, shrunken PR nuclei were found in the outer part of the CT specimens. C) A damaged, displaced ribbon synapse (arrow) in the OPL. D) The OPL consists largely of degenerating and swollen processes and electron dense debris. E) A damaged ribbon synapse (arrow) present in the IPL. F) An intact conventional synapse (arrow) in the IPL. G) CT specimen in which the IPL appears disorganized with large electron dense structures, presumed Müller cell processes, filled with cellular debris. H) CT specimens also display an intact ILM, however the innermost part of the specimen displays a Müller cell process but is otherwise void of cellular material. Scale bars A-B, G 2µm; C-F 0,5µm; H 1µm.

Fig 11: Transmission electron microscopy of 10 DIV adult porcine retinal explants. Layer morphology. A) IRS specimens display intact photoreceptor inner segments (IS) with outer segment ciliae (CL) and a continuous outer limiting membrane (OLM). The photoreceptor cilia appear intact, and the IS mitochondria appear healthy. B) Photoreceptor nuclei (PR) and their processes appear healthy in the IRS specimens. C) A multitude of intact ribbon synapses (arrows) were found at the inner border of the ONL in the IRS specimens. D) Large cell bodies line the culture membrane in the IRS specimens. No Müller cell growth into the membrane could be found. E) CT specimens display subretinal Müller cell growth and severe gliotic remodeling with only a few, shrunken unidentifiable nuclei present. F) Isolated, small photoreceptor nuclei were found in the ONL of CT specimens. G) Müller cell nuclei, and unidentifiable apoptotic nuclei, were present in the INL of CT specimens. H) The inner retina appeared disorganized with dark, Müller cell processes lining the inner border. Scale bars A-B 2µm, C-D 1µm, E-H 5µm.

Fig 12: Illustration of the hypothetical Müller cell structure in the retinal sheet under varying biomechanical conditions. A) Müller cell scaffold in the normal biomechanical en-

vironment of the eye, with the vitreous (vitr) attached to the inner limiting membrane (ILM). The ILM is flat and the Müller cell endfeet line its retinal border. B) Collapsed retinal network structure as seen when the normal biomechanical milieu is disrupted, i.e during retinal detachment or when the retina is dissected free during the standard culture procedure. The Müller cells react by an increased GFAP expression (green). C) The IRS specimens (shown inverted) where the stability of the Müller cell scaffold is restituted by the apposition of the ILM to the non-elastic culture membrane, thereby flattening the stiff inner retinal border structure.

TABLE 1.

Antigen	Antibody name	Target Cell	Species	Dilution	Source	Reference
NeuN (Neuronal Nuclei)	Anti- Neuronal Nuclei	Ganglion cells	Mouse monoclonal	1:100	Millipore, USA	[18]
GS (glutamine Synthetase)	Rabbit anti-GS	Müller cells	Rabbit polyclonal	1:200	Abcam, Cambridge, UK	[52]
bFGF (basic fibroblast growth factor)	Mouse anti-bFGF	Müller cells, displaced amacrine cells	Mouse monoclonal	1:200	Sigma Aldrich, St Louis, MO, USA	[18]
Rhodopsin	Rho4D2	Rod photoreceptor	Mouse monoclonal	1:100	Kind gift of Prof. RS Molday, Vancouver, Canada	[53]
GFAP (glial fibrillary acidic protein	Anti-Glial Fibrillary Acidic Protein	Activated Müller cells, astrocytes	Mouse monoclonal	1:200	Chemicon International, Ca, USA	[18]
Transducin	Anti Transducin Gβ3 (C-16)	Cone photoreceptors, cone bipolar cells	Mouse polyclonal	1:50	Santa Cruz Biotechnology Inc. Dallas, TX, USA	[54]
Synaptophysin	rabbit anti-human synaptophysin protein	Presynaptic vesicles	Rabbit polyclonal	1:100	Dako, Copenhagen, Denmark	[55]
2ndary Antibody	**Antibody name**	**Target**	**Species**	**Dilution**	**Source**	**Reference**
FITC (fluorescein isothiocyanate)	Anti-mouse IgG FITC conjugate	Anti-mouse	Goat	1:200	Sigma Aldrich, St Louis, MO, USA	[18]
Texas red	Texas Red dye-conjugated AffiniPure	Anti-rabbit	Donkey	1:200	Jackson ImmunoResearch, PA, USA	[18]

Table 1. Table of primary and secondary antibodies used for immunohistochemical analysis.

REFERENCES

1. Marmor MF, Yao XY, Hangeman GS. Retinal adhesiveness in surgically enucleated human eyes. Retina. 1994;14:181–186.

2. Franze K, Francke M, Günter K, et al. Spatial mapping of the mechanical properties of the living retina using scanning force microscopy. Soft Matter. 2011;7:3147-3154.

3. Lewis GP, Matsumoto B, Fisher SK. Changes in the organization and expression of cytoskeletal proteins during retinal degeneration induced by retinal detachment. Invest Ophthalmol Vis Sci. 1995;36(12):2404-2416.

4. Winkler J, Hagelstein S, Rohde M, Laqua H. Cellular and cytoskeletal dynamics within organ cultures of porcine neuroretina. Exp Eye Res 2002;74:777–788.

5. Taylor L, Moran D, Arnér K, Warrant E, Ghosh F. Stretch To See - Lateral tension strongly determines cell survival in long-term cultures of adult porcine retina. Invest Ophthalmol Vis Sci. 2013;54(3):1845-1855

6. Lindqvist N, Liu Q, Zajadacz J, Franze K, Reichenbach A. Retinal glial (Müller) cells: sensing and responding to tissue stretch. Invest Ophthalmol Vis Sci. 2010;51:1683-1690.

7. Ryskamp DA, Witkovsky P, Barabas P, et al. The polymodal ion channel TRPV4 modulates calcium flux, spiking rate and apoptosis of mouse retinal ganglion cells. J Neurosci. 2011;31:7089-7101.

8. Tansley K. Formation of rosettes in the rat retina. Br J Opthalmol. 1933;17(6):321-336.

9. Caffé AR, Visser H, Jansen HG, Sanyal S: Histotypic differentiation of neonatal mouse retina in organ culture. Curr Eye Res. 1989;8: 1083–1092.

10. Ogilvie JM. Speck JD, Lett JM, Fleming TT. A reliable method for organ culture of neonatal mouse retina with long-term survival. 1999;87(1):57-65.

11. Ogilvie JM, Speck JD, Lett JM. Growth factors in combination, but not individually, rescue rd mouse photoreceptors in organ culture. Exp Neurol 2000;161:676–685.

12. Engelsberg K, Ghosh F. Transplantation of cultured adult porcine neuroretina. Cell Transpl. 2007;16:31-39.

13. Ghosh F, Taylor L, Arnér K. Exogenous glutamate modulates porcine retinal development in vitro. Dev Neurosci. 2012;34(5):428-39

14. Kaempf S, Walter P, Salz AK, Thumann G. Novel organotypic culture model of adult mammalian neurosensory retina in co-culture with retinal pigment epithelium. J. Neurosci. Methods. 2008;17:47-58.

15. Kobuch K, Herrmann WA, Framme C, Sachs HG, Gabel VP, Hillenkamp J. Maintenance of adult porcine retina and retinal pigment epithelium in perfusion culture: characterisation of an organotypic in vitro model. Exp Eye Res. 2008;86:661–668.

16. Fernandez-Bueno I, Pastor JC, Gayoso JM, Alcalde I, Garcia MT. Müller and macrophage- like cell interactions in an organotypic culture of porcine neuroretina. Mol Vis. 2008;14:2148-2156.

17. Taylor L, Arnér K, Engelsberg K, Ghosh F. Effects of glial cell line-derived neurotrophic factor on the cultured adult full-thickness porcine retina. Curr Eye Res. 2013;38(4);503-515

18. Johansson UE, Eftekhari S, Warfvinge K. A battery of cell- and structure specific markers for the adult porcine retina. J Histochem Cytochem. 2010;58:377-89 20.

19.Wang J, Kolomeyer AM, Zarbin MA, Townes-Anderson E. Organotypic Culture of Full-thickness Adult Porcine Retina. J Vis Exp. 2011;49:2655

20 Dallacasagrande V, Zink M, Huth S, Jakob A, Müller M, Reichenbach A, Käs JA, Mayr SG. Tailoring Substrates for Long-Term Organotypic Culture of Adult Neuronal Tissue. Adv Matter. 2012;24:2399-2403

21. Villegas-Perez MP, Vidal-Sanz M, Rasminsky M, Bray GM, Aguayo AJ. Rapid and protracted phases of retinal ganglion cell loss follow axotomy in the optic nerve of adult rats. J Neurobiol. 1993;24(1):23-36.

22. Berkelaar M, Clarke DB, Wang YC, Bray GM, Aguayo AJ. Axotomy results in delayed death and apoptosis of retinal ganglion cells in adult rats. J Neurosci. 1994;14(7):4368-74.

23. Bonfanti L, Strettoi E, Chierzi S, et al. Protection of retinal ganglion cells from natural and axotomy-induced cell death in neonatal transgenic mice overexpressing bcl-2. J Neurosci. 1996;16(13):4186-94.

24. Cenni MC, Bonfanti L, Martinou JC, Ratto GM, Strettoi E, Maffei L. Long-term survival of retinal ganglion cells following optic nerve section in adult bcl-2 transgenic mice. Eur J Neurosci. 1996;8(8):1735-45.

25. Klöcker N, Bräunling F, Isenmann S, Bähr M. In vivo neurotrophic effects of GDNF on axotomized retinal ganglion cells. Neuroreport. 1997;8(16):3439-42.

26. Johnson JE, Barde YA, Schwab M, Thoenen H. Brain-derived neurotrophic factor supports the survival of cultured rat retinal ganglion cells. J Neurosci. 1986;6(10):3031-8.

27. Cohen A, Bray GM, Aguayo AJ. Neurotrophin-4/5 (NT-4/5) increases adult rat retinal ganglion cell survival and neurite outgrowth in vitro. J Neurobiol. 1994;25(8):953-9.

28. Mey J, Thanos S. Intravitreal injections of neurotrophic factors support the survival of axotomized retinal ganglion cells in adult rats in vivo. Brain Res. 1993;602(2):304-17.

29. Weibel D, Kreutzberg GW, Schwab ME. Brain-derived neurotrophic factor (BDNF) prevents lesion-induced axonal die-back in young rat optic nerve. Brain Res. 1995;679(2):249-54.

30. Cui Q, Yip HK, Zhao RC, So KF, Harvey AR. Intraocular elevation of cyclic AMP potentiates ciliary neurotrophic factor-induced regeneration of adult rat retinal ganglion cell axons. Mol Cell Neurosci. 2003;22(1):49-61.

31. Shen S, Wiemelt AP, McMorris FA, Barres BA. Retinal ganglion cells lose trophic responsiveness after axotomy. Neuron. 1999;23(2):285-95.

32. Fisher SK, Lewis GP. Müller cell and neuronal remodeling in retinal detachment and reattachment and their potential consequences for visual recovery: a review and reconsideration of recent data. Vision Res. 2003;43:887-897.

33. Fisher SK, Lewis GP, Linberg KA, Verardo MR. Cellular remodeling in mammalian retina: results from studies of experimental retinal detachment. Prog Retin Eye Res. 2005;24:395-431.

34. Cook B, Lewis GP, Fisher SK, Adler R. Apoptotic photoreceptor degeneration in experimental retinal detachment. Invest Ophthalmol Vis Sci. 1995;36(6):990-6.

35. Lewis GP, Charteris DG, Sethi CS, Leitner WP, Linberg KA, Fisher SK. The ability of rapid retinal reattachment to stop or reverse the cellular and molecular events initiated by detachment. Invest Ophthalmol Vis Sci. 2002;43(7):2412-20.

36. Wang M, Munch IC, Hasler PW, Prünte C, Larsen M. Central serous chorioretinopathy. Acta Ophthalmol. 2008;86(2):126-45.

37. Reichenbach A, Eberhardt W, Scheibe R, et al. Development of the rabbit retina. IV. Tissue tensility and elasticity in dependence on topo- graphic specializations. Exp. Eye Res. 1991;53:241-251.

38. Yao XY, Hageman GS, Marmor MF. Retinal adhesiveness in the monkey. Invest Ophthalmol Vis Sci. 1994;35:744–748.

39. Lu YB, Franze K, Seifert G, et al. Viscoelastic properties of individual glial cells and neurons in the CNS. PNAS. 2006;103:17759-17764.

40. Bringmann A, Pannicke T, Grosche J, et al. Müller cells in the healthy and diseased retina. Prog Retin Eye Res. 2006;25:397–424.

41. Bringmann A, Iandiev I, Pannicke T, et al. Cellular signaling and factors involved in Müller cell gliosis: Neuroprotective and detrimental effects. Prog Retin Eye Res. 2009;28:423-451.

42. Lu YB, Iandiev I, Hollborn M, et al. Reactive glial cells: increased stiffness correlates with increased intermediate filament expression. FASEB J. 2011;25:624-631.

43. Lewis GP, Erickson PA, Guérin CJ, Anderson DH, Fisher SK. Basic fibroblast growth factor: a potential regulator of proliferation and intermediate filament expression in the retina. J Neurosci. 1992;12(10):3968-78.

44. Phan MN, Leddy HA, Votta BJ, et al. Functional characterization of TRPV4 as an osmotically sensitive ion channel in porcine articular chondrocytes. Arthritis Rheum. 2009;60:3028-3037.

45. Loukin S, Zhou X, Su Z, Saimi Y, Kung C. Wild-type and brachyolmia-causing mutant TRPV4 channels respond directly to stretch force. J Biol Chem. 2010;285:27176–27181.

46. Sackin H. Stretch-activated ion channels. Kidney Int. 1995;48:1134–1147.

47. Vollrath MA, Kwan KY, Corey DP. The micromachinery of mechanotransduction in hair cells. Annu Rev Neurosci. 2007;30:339-365.

48. Cooper KE, Tang JM, Rae JL, Eisenberg RS. A cation channel in frog lens epithelia responsive to pressure and calcium. J Membr Biol. 1986;93:259-269.

49. Mintenig GM, Sánchez-Vives MV, Martin C, Gual A, Belmonte C. Sensory receptors in the anterior uvea of the cat's eye. An in vitro study. Invest Ophthalmol Vis Sci. 1995;36:1615-1624.

50. Hauck SM, Suppmann S, Ueffing M. Proteomic profiling of primary retinal Müller glia cells reveals a shift in expression patterns upon adaptation to in vitro conditions. Glia. 2003;44: 251–263.

51. García M, Forster V, Hicks D, Vecino E. Effects of Müller glia on cell survival and neuritogenesis in adult porcine retina in vitro. Invest Ophthalmol Vis Sci. 2002;43:3735-3743.

52. Ahn M, Moon C, Jung C, Kim H, Jin JK, Shin T. Immunohistochemical localization of protein kinase C-alpha in the retina of pigs during postnatal development. Neuroscience Letters. 2009;455:93–96.

53. Khodair MA, Zarbin MA, Townes-Anderson E. Synaptic plasticity in mammalian photoreceptors prepared as sheets for retinal transplantation. Invest Ophthalmol Vis Sci. 2003;44:4976-4988.

54. Lobanova ES, Finkelstein S, Herrmann R, et al. Transducin γ-subunit sets expression levels of α- and β-subunits and is crucial for rod viability. Neurosci. 2008;28:3510-3520.

55. Wiedemann B, Franke WW. Identification and localization of synaptophysin, an integral membrane glycoprotein of Mr 38,000 characteristic of presynaptic vesicles. Cell. 1985;41:1017-1028.

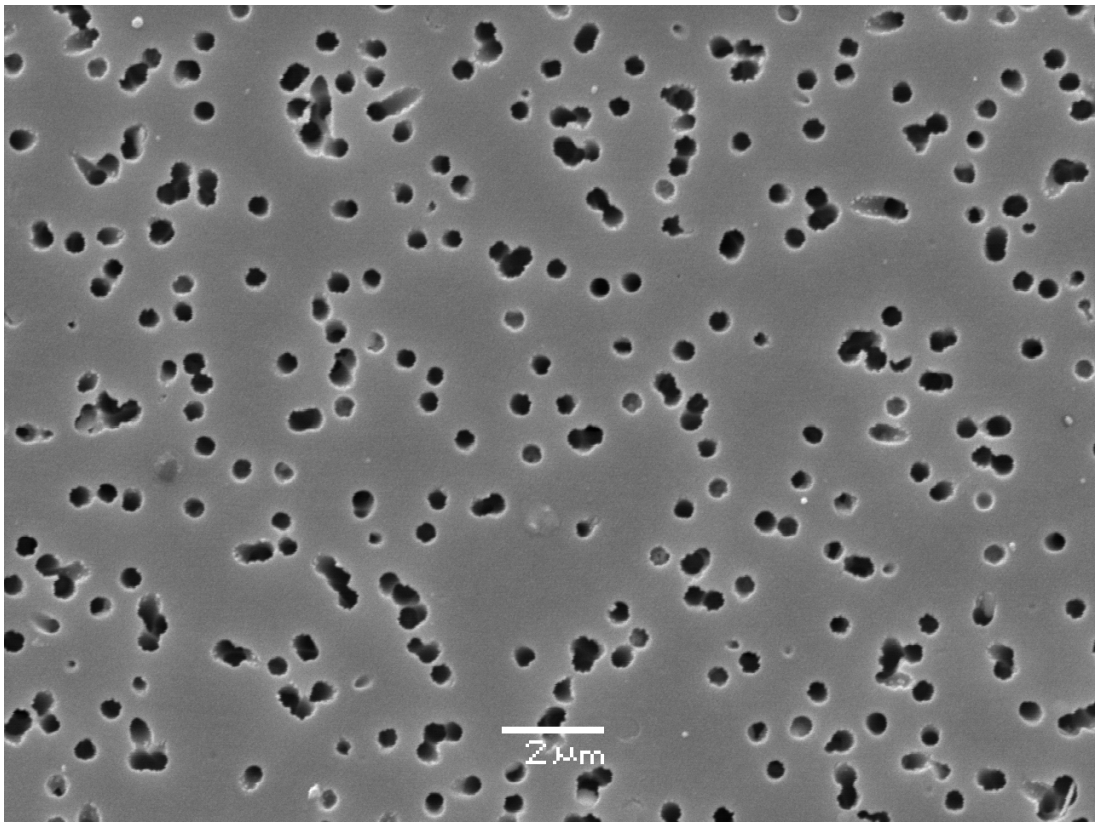

Figure 1. Taylor et al., 2013

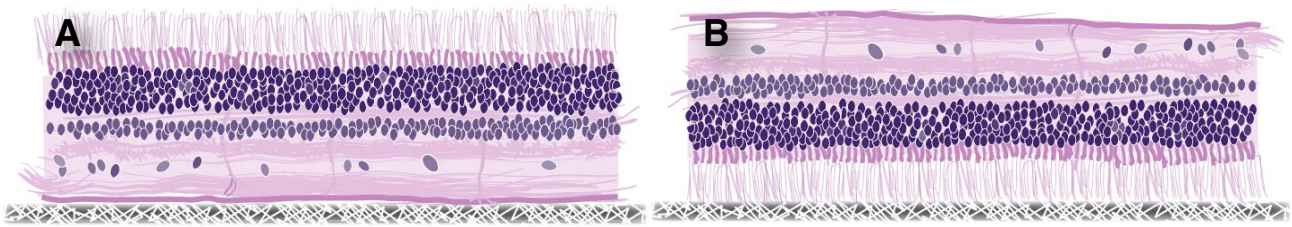

Fig. 2. Taylor et al., 2013

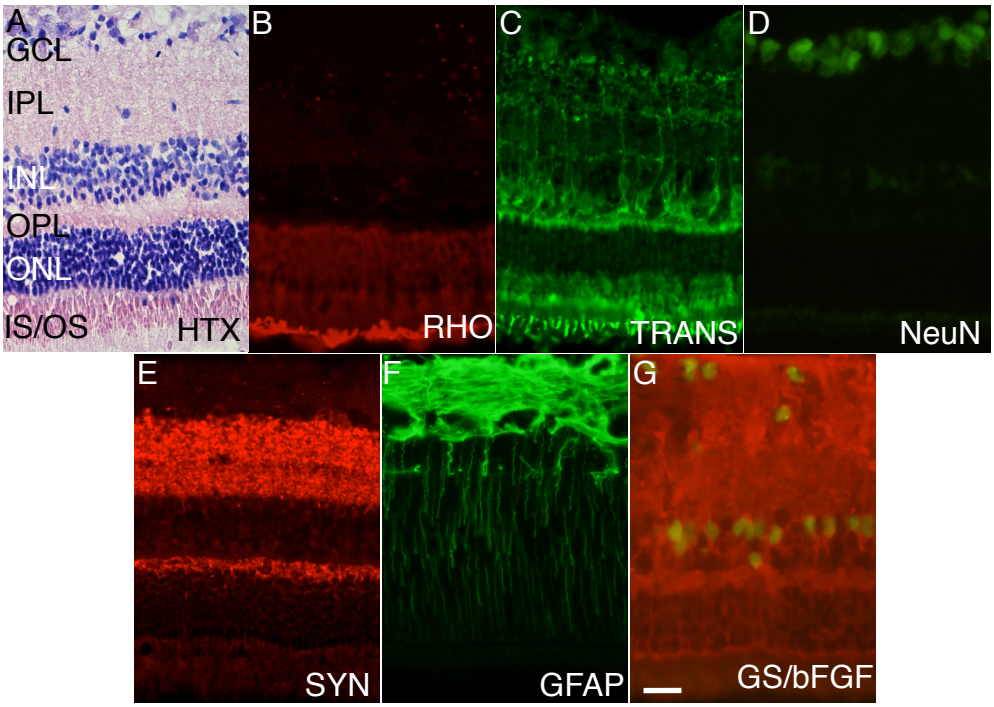

Figure 3. Taylor et al., 2013

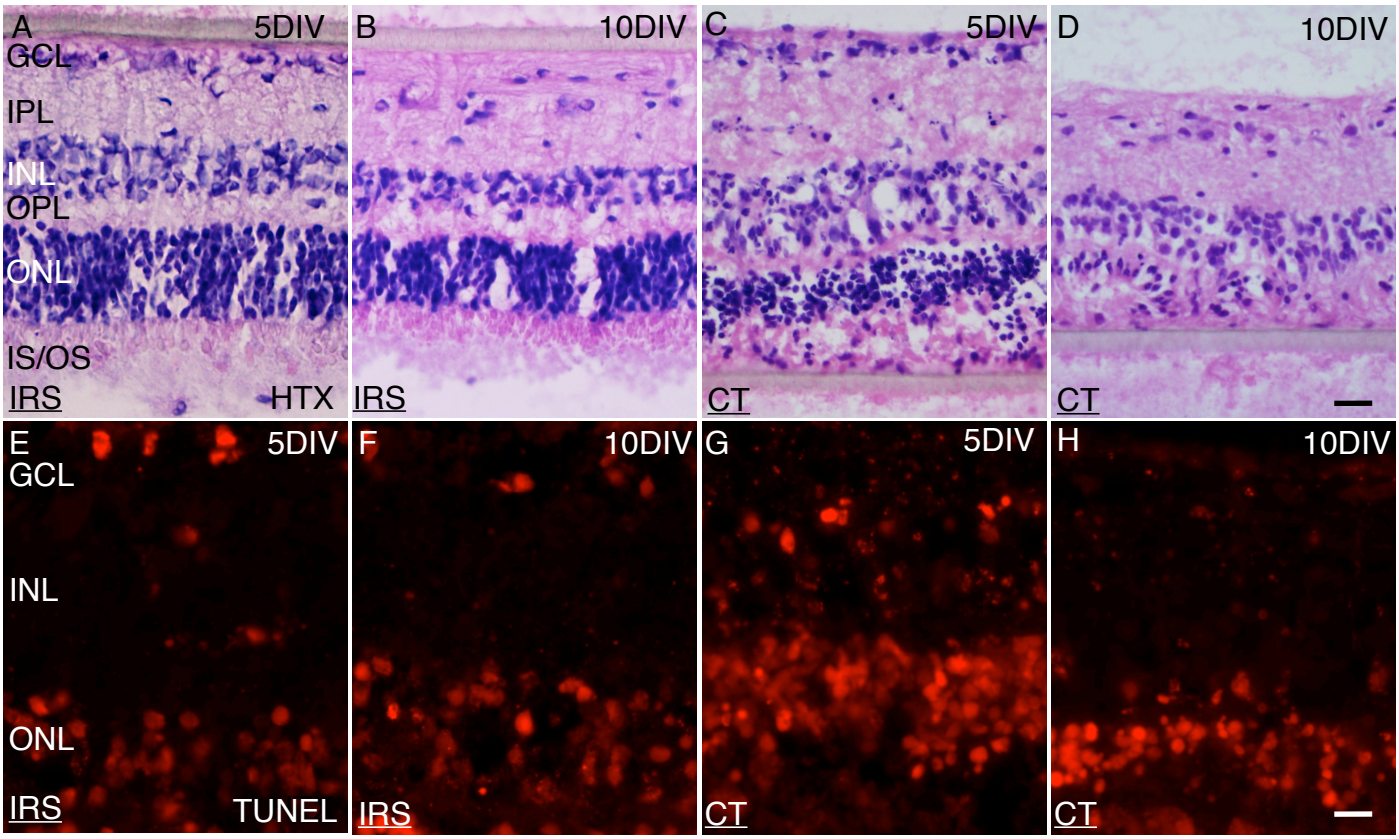

Figure 4. Taylor et al., 2013

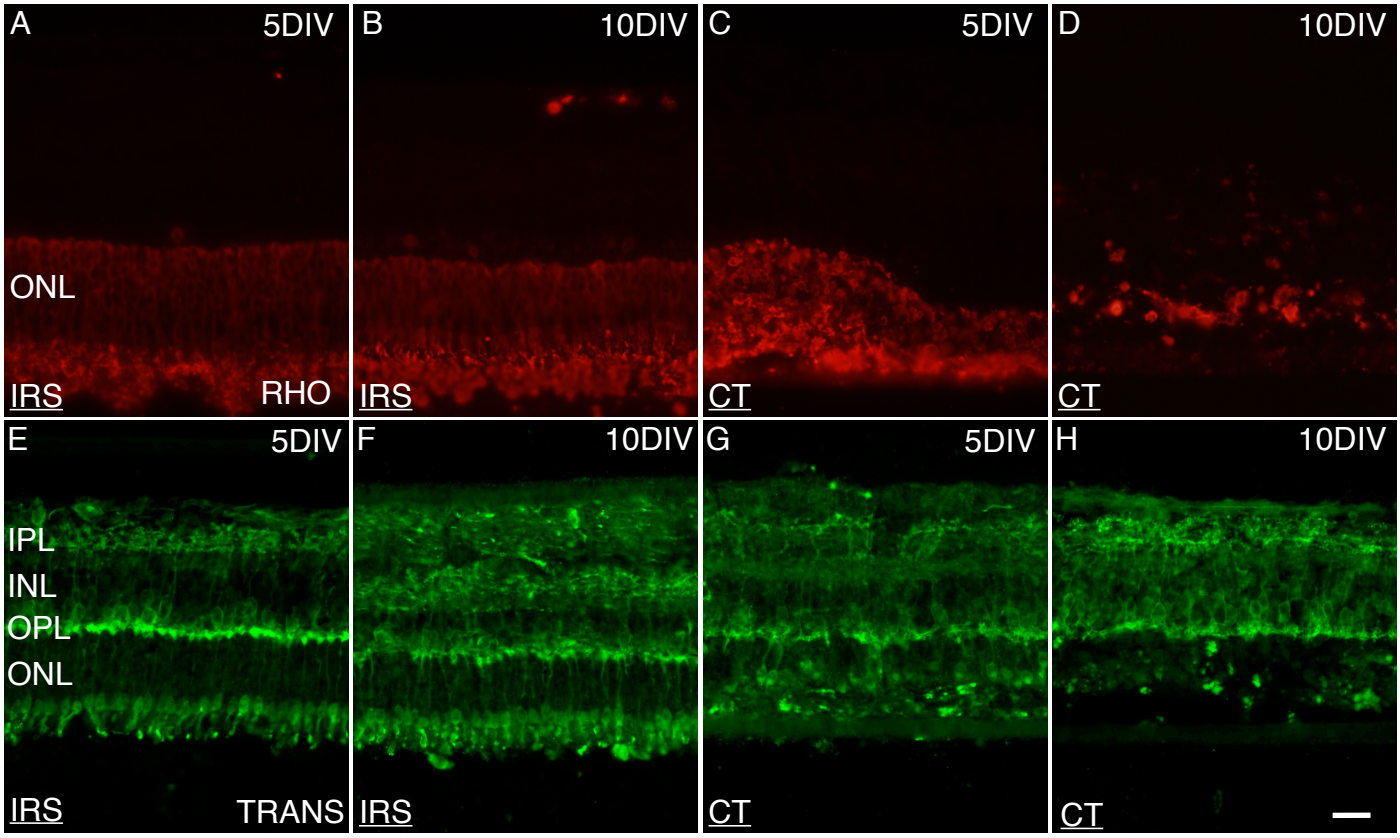

Figure 6. Taylor et al., 2013

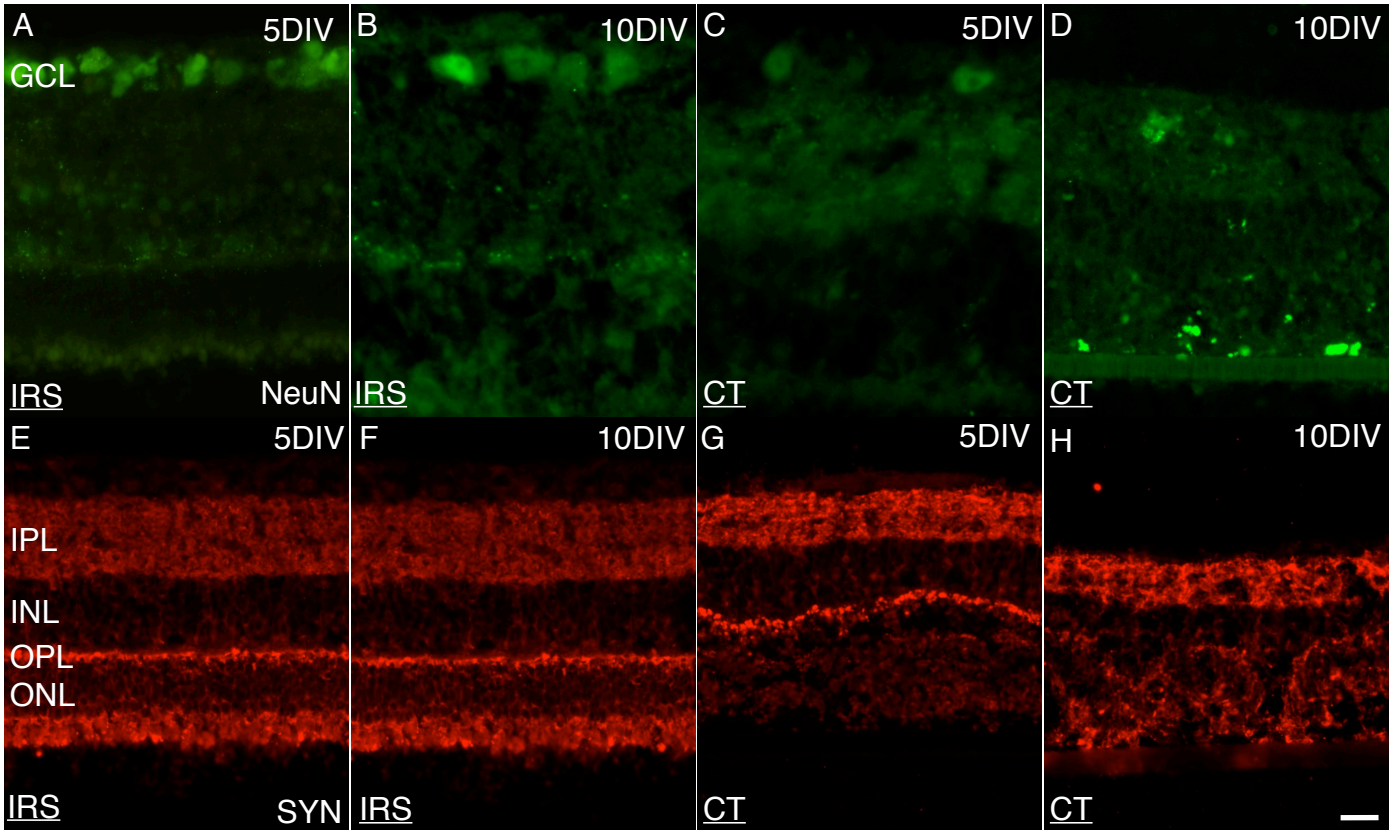

Figure 7. Taylor et al., 2013

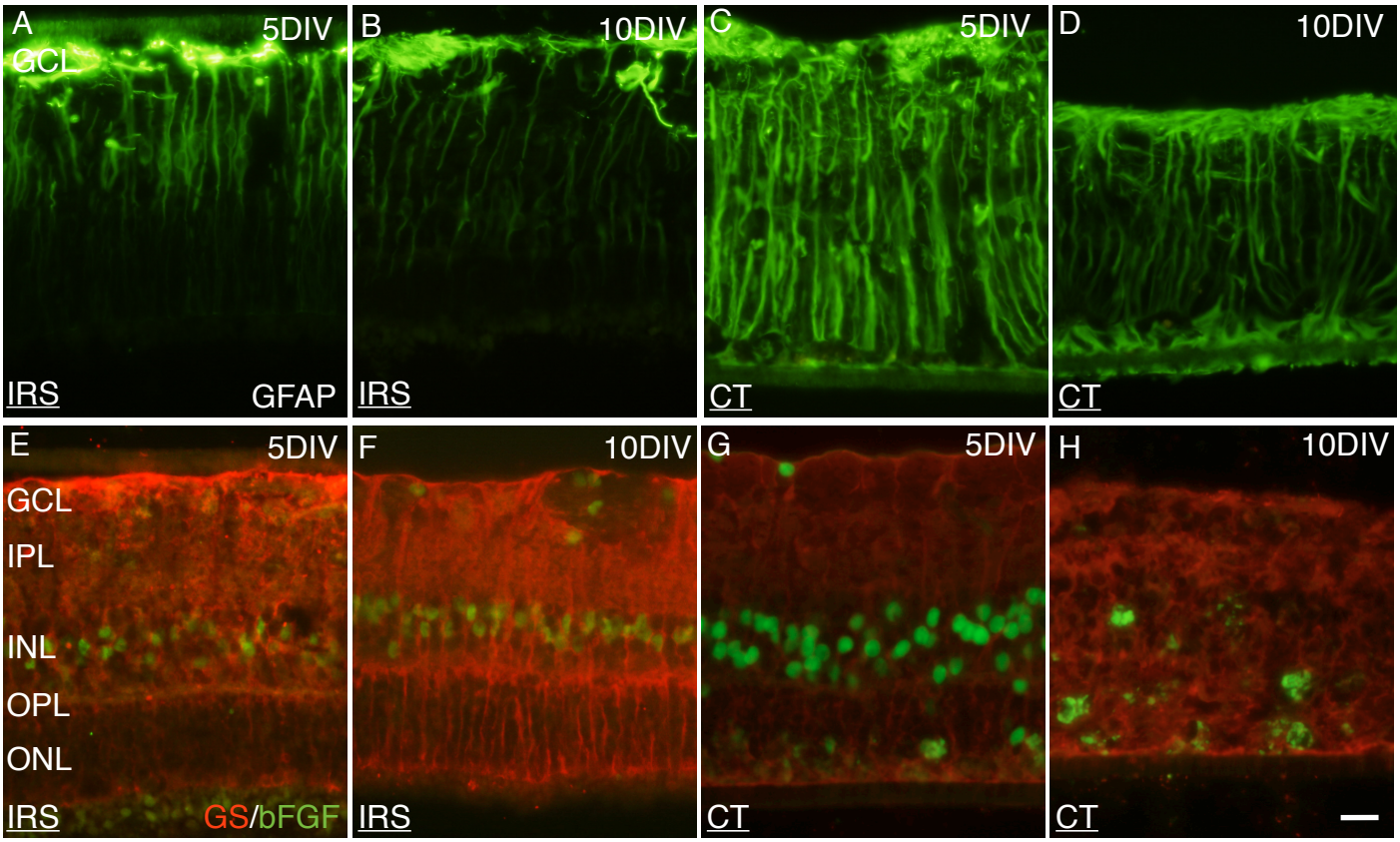

Figure 8. Taylor et al., 2013

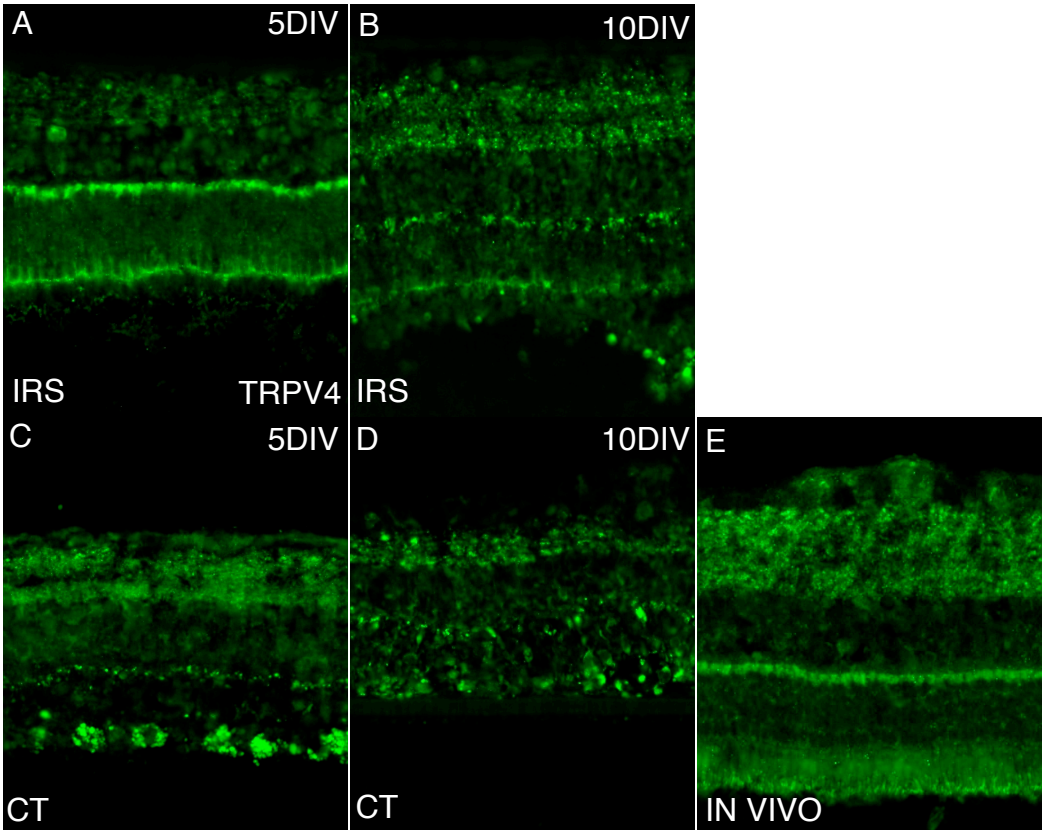

Figure X. Taylor et al., 2013

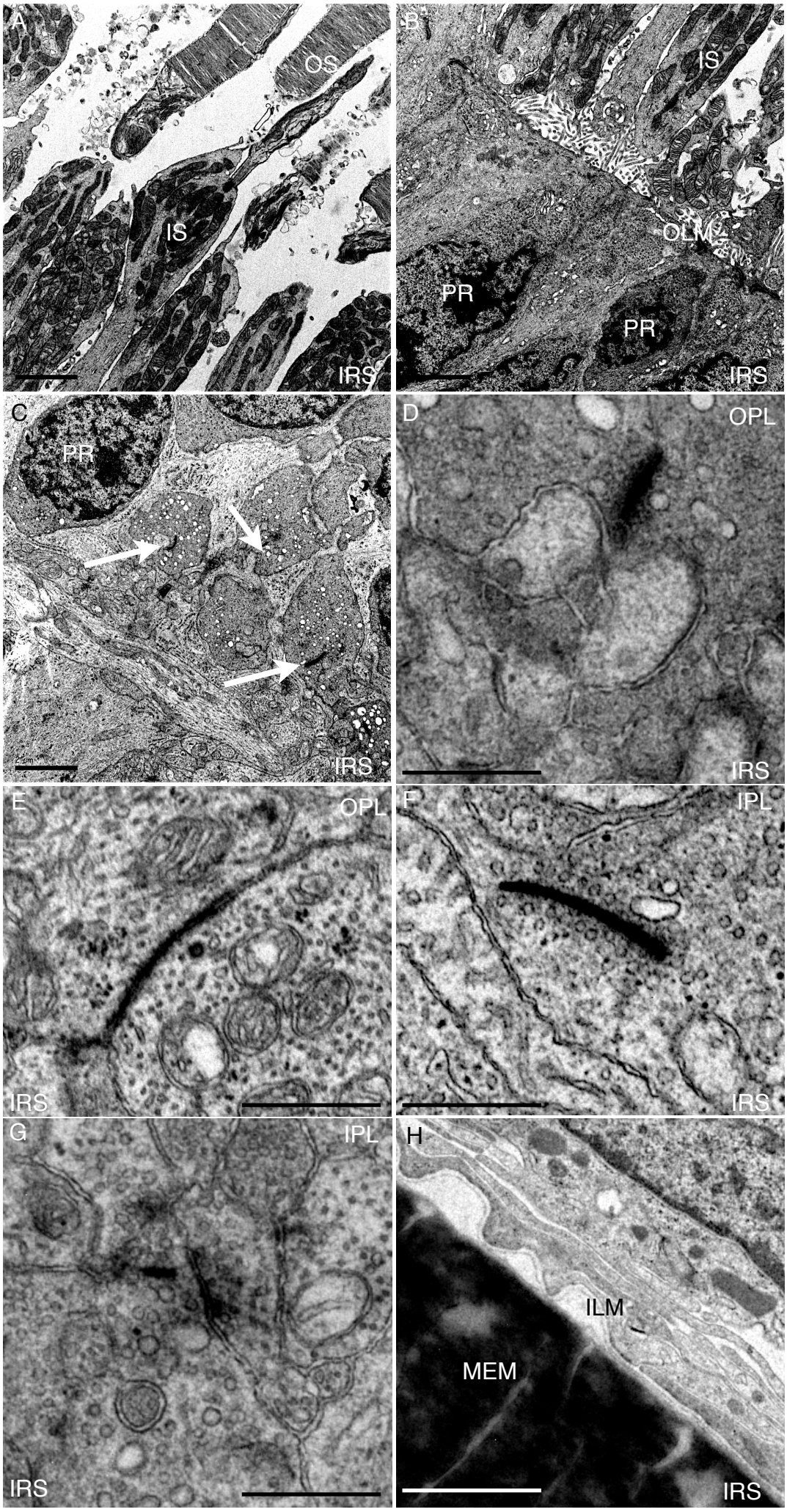

Figure 9. Taylor et al., 2013

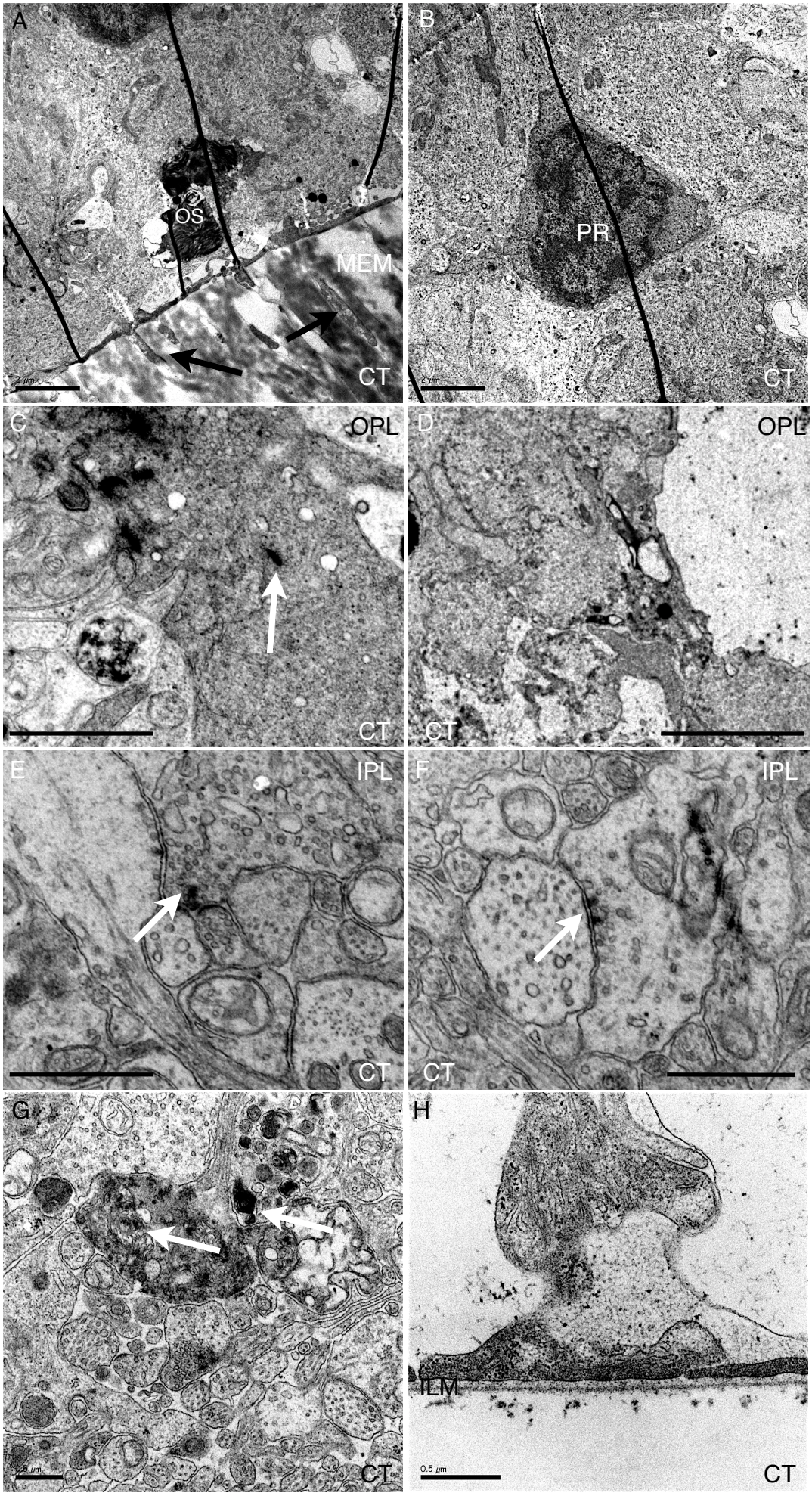

Figure 10. Taylor et al., 2013

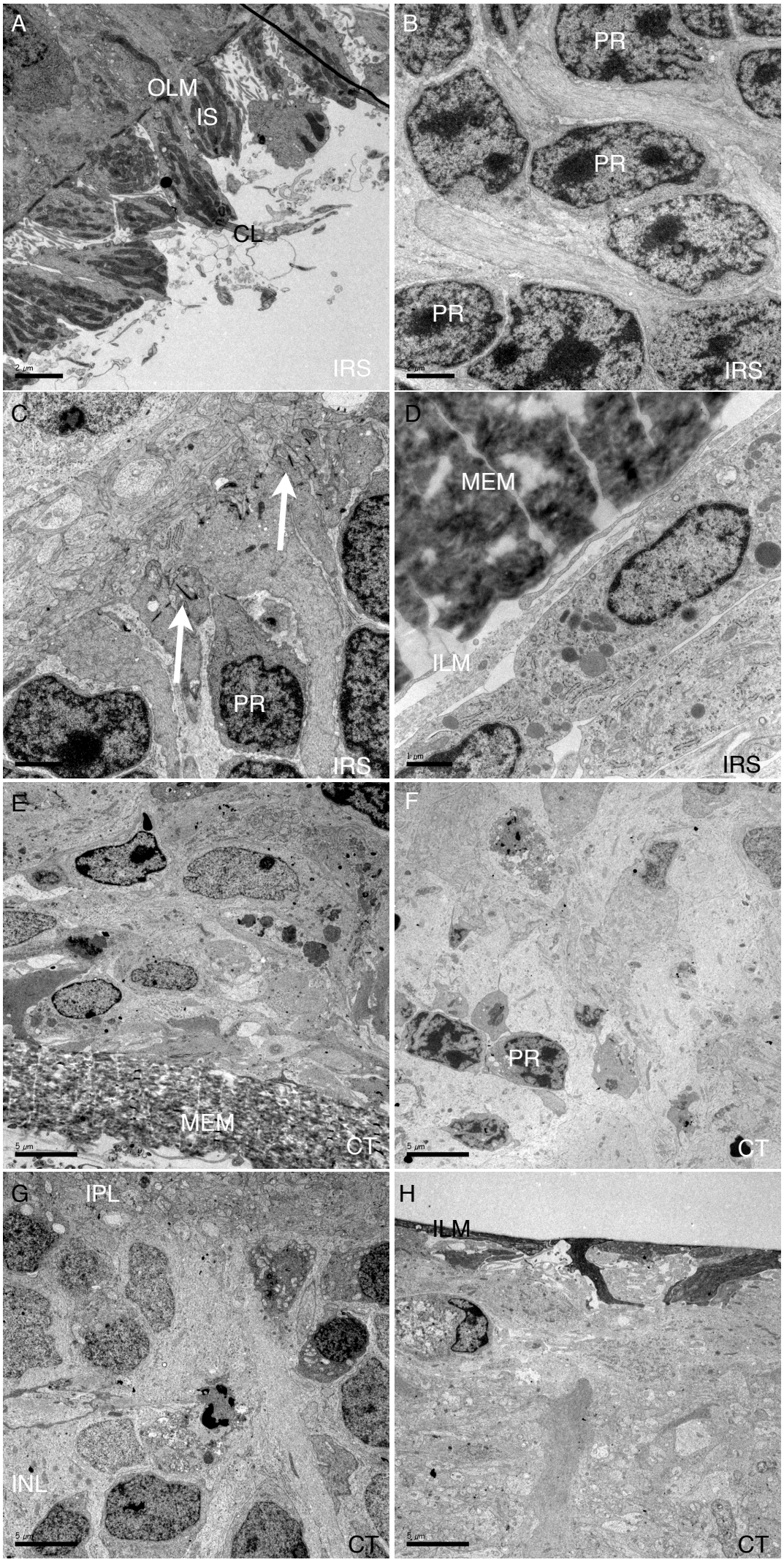

Figure 11. Taylor et al., 2013

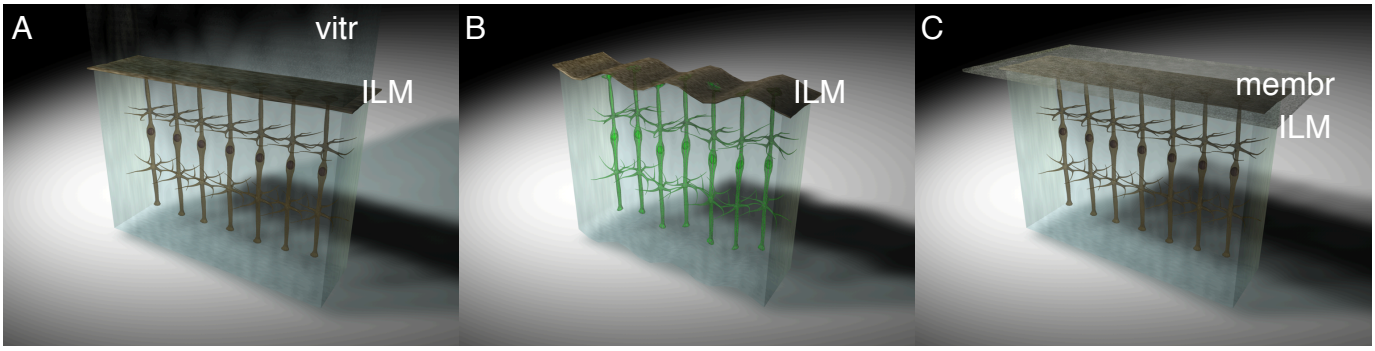

Figure 12. Taylor et al., 2013